ACS APPLIED MATERIALS & INTERFACES

Research Article

www.acsami.org

Shape-Switching Microrobots for Medical Applications: The Influence of Shape in Drug Delivery and Locomotion

Stefano Fusco,[†] Hen-Wei Huang,[†] Kathrin E. Peyer,[†,#] Christian Peters,[‡] Moritz Häberli,[†] André Ulbers,[†] Anastasia Spyrogianni,[§] Eva Pellicer,[∥] Jordi Sort,[*,⊥] Sotiris E. Pratsinis,[§] Bradley J. Nelson,[†] Mahmut Selman Sakar,[*,†] and Salvador Pané[†]

[†]Institute of Robotics and Intelligent Systems, ETH Zürich, Tannenstrasse 3, 8092 Zurich, Switzerland

[‡]Micro and Nanosystem Group, ETH Zürich, Tannenstrasse 3, 8092 Zurich, Switzerland

[§]Particle Technology Laboratory, ETH Zürich, Sonneggstrasse 3, 8092 Zurich, Switzerland

[∥]Departament de Física, Universitat Autònoma de Barcelona, E-08193 Bellaterra, Spain

[⊥]Institució Catalana de Recerca i Estudis Avançats (ICREA) and Departament de Física, Universitat Autònoma de Barcelona, E-08193 Bellaterra, Spain

[#]Faculty of Life Sciences, University of Manchester, Michael Smith Building, Manchester, M13 9PT, United Kingdom

Supporting Information

ABSTRACT: The effect of dynamic shape switching of hydrogel bilayers on the performance of self-folding microrobots is investigated for navigation in body orifices and drug release on demand. Tubular microrobots are fabricated by coupling a thermoresponsive hydrogel nanocomposite with a poly(ethylene glycol)diacrylate (PEGDA) layer, to achieve spontaneous and reversible folding from a planar rectangular structure. Graphene oxide (GO) or silica-coated superparamagnetic iron oxide nanoparticles are dispersed in the thermoresponsive hydrogel matrix to provide near-infrared (NIR) light sensitivity or magnetic actuation, respectively. The NIR light-responsive microstructures are fabricated for triggered drug delivery while magnetic nanocomposite-based microrobots are used to analyze the role of shape in locomotion. Experimental analysis and computational simulations of tubular structures show that drug release and motility can be optimized through controlled shape change. These concepts are finally applied to helical microrobots to show a possible way to achieve autonomous behavior.

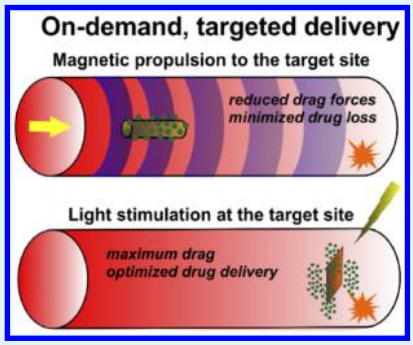

KEYWORDS: *hydrogel nanocomposites, self-folding bilayers, drug delivery, magnetic manipulation, microrobotics*

1. INTRODUCTION

While it is widely accepted that physical and chemical properties of materials play a major role in the interactions between miniaturized biomaterials and the biological environment,[1−5] the influence of shape has not yet been thoroughly examined due to earlier limitations in manufacturing processes. With recent advances in micro- and nanofabrication, several complex architectures with different geometries have been fabricated out of metals, alloys, polymers, ceramics, or combinations thereof.[6] This opened up the opportunity to investigate the role of shape in the interaction between the biological environment and miniaturized biomaterials. For example, recent data have shown that particle geometry significantly influences the intracellular uptake mechanisms and kinetics. Particles with high local curvatures are internalized more easily than those exhibiting flat or concave regions.[7,8] Cylindrical micelles remain in the blood flow longer than their spherical counterparts because hydrodynamic forces on elongated micelles overcome phagocytic forces.[9,10] Moreover, nonspherical particles under capillary hydrodynamic conditions tend to translate and adhere better to vessel walls.[11] Microorganisms use shape switching as an adaptation strategy and exhibit specific morphologies better suited to their lifestyles or transform their shapes in response to external factors. For example, certain types of bacteria can change their shape to fight shear forces when they are subject to an aqueous flow.[12]

The properties of a biomedical platform conferred by a certain shape can be used to target specific organs and regulate their body distribution.[13] Promising material candidates for shape-shifting devices are stimuli-responsive polymers.[14] These materials can naturally modify their physical properties in response to environmental triggers such as pH, temperature, or chemical concentration gradients. Stimuli-responsive hydrogels also exhibit the ability to change their shape and volume depending on environmental conditions.[15] The majority of hydrogel formulations are biocompatible and mechanically deformable. Moreover, their synthesis is highly versatile and can be readily modified to tune the physicochemical attributes of

Received: January 12, 2015
Accepted: March 9, 2015
Published: March 9, 2015

 © 2015 American Chemical Society

DOI: 10.1021/acsami.5b00181
ACS Appl. Mater. Interfaces 2015, 7, 6803−6811

the material composition.[16] Recently, hydrogels have been employed to fabricate shape-switching self-folding bilayer platforms for applications such as targeted drug delivery, tissue engineering, or wireless microsurgery.[17−23] These structures have been successfully miniaturized to generate microrobots that are remotely controlled using magnetic and optical manipulation systems.[24−26]

In this work, we illustrate the potential of self-rolling hydrogel bilayers for fabrication of shape-switching microrobots for applications in targeted drug delivery. We show that by changing the shape, these microrobots can adapt to maximize their performance in terms of drug delivery or locomotion. The tubular shape of a closed bilayer can be beneficial to limit spontaneous drug diffusion during the journey of the platform to its target location and to minimize the interactions with the surrounding fluids. Moreover, tubular shapes exhibit relatively lower drag forces than planar configurations with the same volume. Once the target position is achieved, a rectangular conformation is more convenient since it can be used to increase both the drag forces and the drug release due to an increase in the surface area. These features are initially analyzed with two different types of hydrogel-based bilayers. Hydrogel nanocomposites containing silica-coated iron oxide nanoparticles (γ-Fe_2O_3) are used to produce magnetic microtubes that can be steered by means of an electromagnetic manipulation system.[25] Moreover, a finite element analysis of the drag forces involved in the open (rectangular planar) or closed (tubular) state is provided. The influence of shape on drug delivery is demonstrated using hydrogel bilayers containing graphene oxide (GO) nanoparticles, which can be optically stimulated using near-infrared light (NIR). Diffusion-driven release of brilliant green (BG), a model drug, is analyzed for both open and closed configurations in bilayers, and their performance is compared to that of single layer GO nanocomposites. A finite element model is also developed to analyze the effect of shape changes on drug release. Finally, a helical magnetic soft microrobot that changes shape depending on the environmental temperature is presented. Using magnetic helical microstructures, rotating uniform magnetic fields can be transduced into forward motion.[28] The robots can regulate their motility by sensing their microenvironment (in this case, temperature) and show autonomous behavior.

2. EXPERIMENTAL SECTION

2.1. Materials. *N*-Isopropylacrylamide monomer (NIPAAM), acrylamide (AAM), poly(ethylene glycol) diacrylate (average MW 575, PEGDA), 2,2-dimethoxy-2 phenylacetophenone (99%, DMPA), ethyl lactate (98%, EL), anhydrous hexane (95%) were purchased from Sigma-Aldrich (St. Louis, MO). 1*H*,1*H*,2*H*,2*H*-Perfluorodecyltrichlorosilane (PFDTCS) and graphite powder were purchased from ABCR (Germany). The main NIPAAM monomer was recrystallized after double treatment in *n*-hexane solution, while all other chemicals were used as received. SU-8 photoresist and developer and Lift-Off Resist (LOR), used as a sacrificial layer, were purchased from MicroChem (Westborough, MA), while AZ 4562 photoresist and AZ 826 developer where purchased from Clariant (Germany). Silica (23 wt %)-coated γ-Fe_2O_3 particles were produced by spray pyrolysis, as described previously.[34] For their synthesis, iron(III) acetylacetonate ($Fe(acac)_3$, purum, ≥97.0%), xylene (puriss. p.a., ACS reagent), acetonitrile (ACS reagent, ≥99.5% and hexamethyldisiloxane (HMDSO, puriss, ≥98.5%) were purchased from Sigma-Aldrich.

2.2. GO Synthesis. GO sheets were synthesized from natural graphite powder, by a modified Hummers Method.[49] First, 3 g of graphite (0.25 mol) and 3.6 g of $NaNO_3$ (~0.05 mol) were mixed in concentrated H_2SO_4 (~150 mL), and the mixture was cooled to 4 °C by immersion in a water/ice bath. After 30 min, 18 g of $KMnO_4$ (~0.10 mol) were slowly added under vigorous stirring, producing a slight exotherm to 35−40 °C. This temperature was maintained, and the reaction of oxidation kept going under stirring for 7 h, in which an increase in viscosity of a brown−gray solution was observed. Following that, water (150 mL) was slowly added, producing a large exotherm to 95 °C. The dilute suspension, brown in color, was stirred for 30 min and then further diluted with 200 mL of water and 6 mL of H_2O_2 (30%) to reduce and solubilize the residual permanganate. Upon this treatment, the solution turned a light yellow color. The diluted suspension was stirred for an additional 16 h, after which it was filtered, and the solid product was washed repetitively with diluted HCl and water, until the pH reached neutral values. The product was then dried in vacuum and exfoliated in nanosheets by ultrasonication to produce a highly stable water dispersible powder.

2.3. Fabrication of Hydrogel Bilayers. The rolled microstructures are the result of a two-step, backside exposure photolithographic process where two different layers were subsequently created without employing any alignment on a glass photomask. Thickness of the layers was controlled by using SU-8 spacers previously fabricated on the bottom silicon substrate. The masks were designed on plastic foil (Selba S.A., Switzerland) and reproduced on glass wafers by photolithography using the positive photoresist AZ4562. For these experiments, squares with the side of 3 mm were used as two-dimensional (2D) shapes. A 100 nm chromium layer was evaporated on the substrates and removed from the features areas by rinsing the photoresist from below with acetone and isopropanol. The final masks were then coated with an LOR sacrificial adhesive layer to provide a uniform adhesion of the hydrogel layers. SU-8 spacers of different thickness (1.5−40 μm, as measured by surface profilometry) were prepared by photolithography on SiO_2 substrates. A nonadhesive layer based on PFDTCS was added by vapor silanization overnight and activated at 90 °C to prevent adhesion of hydrogels.

After the mask was placed on a 10 μm thick spacer substrate, a hydrogel solution composed of PEGDA with 3 wt % DMPA photo initiator and 50 wt % ethyl lactate was infiltrated by capillarity into the photopolymerization cell and polymerized at 365 nm for 2 min (300 W mercury lamp, 4 mJ/cm^2, Karl Süss Microtec, Germany). After separating the two substrates the hydrogels remained attached to the mask side ensuring the possibility for a second polymerization step. A NIPAAM−AAM−PEGDA (molar ratio 85/15/0.4) solution, with 3 wt % DMPA photoinitiator, 70 wt % ethyl lactate was used for the responsive layer production. Depending on the final application, GO (3 wt %) or silica-coated γ-Fe_2O_3 nanoparticles (0.1, 1, 2, 4, and 8 wt % were considered to find the values suitable for manipulation of the final devices) were added and dispersed into the solution by ultrasonication (4000 J, by means of a probe sonicator, SONICS, Newtown, CT). The nanocomposite solution was introduced into the space between the photomask and a 40 μm thick spacer substrate, after the PEGDA solution that was not polymerized solution was carefully removed. Polymerization was carried out for an additional 3 min in case of graphene oxide, and 6 min for the magnetic nanocomposite. After UV curing, the cell was opened, and the bilayers attached to the mask were released through immersion in water.

2.4. Fabrication of Hydrogel Single Layers. Hydrogel layers of NIPAAM−AAM−PEGDA (molar ratio 85/15/0.4) with 3 wt % GO, used for drug delivery experiments were fabricated by photo polymerization (3 min at 365 nm) in between two 4 in. glass wafers, separated by 180 μm thick glass spacers. The layers were allowed to swell and spontaneously detached from the glass slides. After that, round shaped samples (3 mm diameter) were taken by using a disposable biopsy punch (Schuco, Watford, United Kingdom), deeply rinsed, and kept in ultrapure water. The same method was used to produce single layers of iron oxide nanocomposites for characterization of the magnetic performance.

2.5. Characterization of the Magnetic Nanoparticles. The specific surface area (SSA) of the synthesized silica-coated Fe_2O_3 particles was measured by N_2 adsorption at 77 K using a five-point Brunauer−Emmet−Teller (BET) method (Tristar 3000, Micrometrics) after degassing the samples for at least 1 h at 150 °C in

DOI: 10.1021/acsami.5b00181
ACS Appl. Mater. Interfaces 2015, 7, 6803−6811

nitrogen. The particle SSA was 66 ± 7 m^2/g, as determined by 4 independently synthesized samples, in excellent agreement with previous work.[34] Using the particle SSA and an average particle density, the equivalent average primary particle diameter was determined to be 24.1 ± 2.6 nm (see Supporting Information for equation), which is consistent with the previously reported count mean diameter of 22.9 nm for such particles determined by electron microscopy images.[34] The dispersibility of the suspensions in ethyl lactate, the solvent used for the described experiments, was estimated by measuring size distributions by dynamic light scattering (DLS, Zetasizer nano series, Malvern Instruments, Ltd., Malvern, United Kingdom). The suspensions were prepared by dispersing 130 mg of silica-coated Fe_2O_3 (8 wt %) in 1 mL of ethyl lactate and then sonicating them with a water-cooled high-intensity cup horn system (VCX500, cup horn, part no. 630−0431, Sonics Vibracell). The total liquid volume (volume of the cooling water plus suspension volume) was approximately 0.5 L and 500 kJ of ultrasonic dispersion energy was provided in pulses (30 s on, 1 s off) at 95% amplitude. The resultant solution was diluted 200 times to allow DLS analysis. The measured intensity distributions allowed estimating the number distribution and the average agglomerate hydrodynamic size.

2.6. Characterization of the Hydrogel Magnetic Nanocomposites. Magnetic nanocomposites were characterized in terms of swelling and magnetic properties. Swelling experiments were performed to understand the influence of the high concentration of nanoparticles on the hydration of the samples. Sections of gels of the magnetic thermo responsive layers (a minimum of 3 per type) were polymerized, rinsed in ultrapure water, dried, and then allowed to swell in water. Their dried (M_d) and swollen (M_s) weights were recorded and the equilibrium swelling ratio (ESR) defined as (eq 1):

$$\mathrm{ESR} = \frac{M_s - M_d}{M_d} \tag{1}$$

The result was compared to previous analysis of the hydrogel composition without the nanoparticles. Magnetic hysteresis loops of the nanocomposites were measured using a vibrating sample magnetometer (VSM, Oxford Instruments 1.2, United Kingdom) by applying a magnetic field in the range between −1 and 1 T, at room temperature. The morphology of the films was imaged by Cryo-SEM.

2.7. Drug Delivery Experiments. Cylindrical hydrogel bilayers (square of 3 mm) were rinsed for 24 h after fabrication to wash away the unreacted materials, then they were dried and subsequently immersed in a 1 mM BG solution in PBS. They were allowed to swell for a total time of 24 h, subsequently dried for 30 min and immersed in deionized (DI) water for 1 min to rinse the dye on the surface. Following these preparation steps, some of them were immersed in 300 μL of PBS, and the release of the BG embedded in the hydrogel matrices was monitored at room temperature for a period of 1 month. At defined times, the solvent was collected and measured by UV−vis spectroscopy (Infinite M200 Pro, Tecan AG, Mannendorf, Switzerland) at 624 nm wavelength and replaced with fresh solution (in order to mimic a perfect sink condition). Release kinetics was evaluated by fitting the in vitro data to different empirical models using MATLAB (The mathworks, Natick, MA). Similarly, a set of 3 samples was prepared and exposed for the first 2 h to continuous NIR laser light (wavelength 785 nm, 1.5 W power, laser spot 5 mm, SLOC lasers, China) to force them to stay in an open configuration. The effect on the cumulative release was monitored in a way similar to the one described above. Additionally, a set of samples was exposed to short ON−OFF cycles of NIR laser light in order to switch between open and closed configuration in a short time range (roughly 2 min). Experiments of continuous exposure to NIR light were performed on single layers of the same light-responsive material (1 mm thick, 3 mm diameter discs) and compared to control samples. Release was monitored for a total period of 2 months. Statistical analysis of variance between the set of samples was performed with the one way ANOVA function of MATLAB (The Mathworks, Natick, MA).

2.8. Magnetic Manipulation of the Hydrogel Bilayers. Automated three-dimensional (3D) locomotion of the magnetic nanocomposite bilayers was achieved by means of the Octomag, a five degree-of-freedom (5-DOF) electromagnetic manipulation setup.[27] The system consists of eight stationary electromagnets with soft magnetic cores capable of generating multiple types of state of the art magnetic control techniques under closed-loop control with computer vision or visual feedback of a human operator.

2.9. FEM Analysis of the Behavior of the Microstructures. We performed 3D finite element analysis of the drug release from folded and unfolded hydrogel tubes by using the commercial software Comsol Multiphysics 4.3b (Comsol, Inc., Burlington, MA). Fick's law of diffusion was used as the governing law for the process. A hollow cylinder resembling the real dimension of the samples (external radius 0.3 mm, internal radius of 0.14 mm, length 2.5 mm) and an open patch (square with size of 2.5 mm) were used as models, and a concentration of 1 mol/m^3 was fixed as an initial condition in the bilayers. Additionally, we considered a third model of a full cylinder with the same volume as the first two. The structures were set into a cubic cell with a side length of 5 mm whose initial external concentration was set to zero. The boundaries of the cubic volume of the model were set to no flux conditions. Diffusion across the boundary between the two gels was assumed to be unobstructed. The diffusion coefficient of brilliant green in water and hydrogels was set to the arbitrary values of 1×10^{-9} cm^2/s and 4.44×10^{-15} cm^2/s (suitable diffusion coefficients for small molecules) for both systems. The simulation was carried out for 1 month, and the concentration accumulated in the water volume was compared. More information about the model can be found in the Supporting Information.

Simulation of the drag forces acting on the hydrogel microrobots in the folded and unfolded state in the 6 relevant coordinates (3 translations in x, y, z, 3 rotations in x, y, z) was compiled by using the same platform (Comsol 4.3b, Inc., Burlington, MA) and the creeping flow interface, based on the Stokes flow equation. The model was built considering a cubic volume with the microstructure positioned in the middle of the space. A constant flow in the z direction of 1 μm/s constituted the simulated relative velocity of the device (the value was chosen to achieve a low Reynolds number regime). The drag forces were calculated according to the theory reported in previous works.[50,51] Briefly, to manipulate arbitrarily shaped microrobots, the orientation dependent microrobot dynamics is evaluated according to eq 2:

$$\vec{F}_{mag} + \vec{F}_{drag} + \vec{F}_g = m\vec{a} \tag{2}$$

where F_{mag} is the magnetic force, F_{drag} is the drag force, and F_g is the gravitational force acting on the microrobot and influencing its acceleration, a. At low Reynolds number the drag force is linear (eq 3):

$$\vec{F}_{drag} = -D^*\vec{v} \tag{3}$$

where D^* is the matrix of drag constants, and v is the relative velocity between the body and the fluid. D depends on the geometrical properties of the body, and the coordinate frame in which the drag force is computed.[52]

3. RESULTS AND DISCUSSION

3.1. Fabrication of Magnetically and NIR Light Responsive Microtubes. A flexible and highly reproducible double-step photolithographic process[29] was used to fabricate hydrogel bilayers. The final 3D shape of the folded structures can be controlled by modulating the 2D pattern printed on the glass mask and the hydrogel layers thickness. Although it is possible to fabricate a large variety of structures with different shapes and sizes,[30] this work is focused on cylindrical tubes generated from the folding of rectangular microstructures. These two geometries were chosen because they have distinct advantages for predetermined tasks (i.e., controlled drug release or magnetic actuation). First, the rolled-up cylinder has a lower surface-to-volume ratio, compared to the unfolded state, thus decreasing the undesired drug release while it is guided toward

DOI: 10.1021/acsami.5b00181
ACS Appl. Mater. Interfaces 2015, 7, 6803−6811

its target location. At the target site, the unfolded rectangular form increases the exposed surface and, therefore, the diffusion-driven release. Second, cylindrical shapes exhibit high magnetic shape anisotropy, that is, they are aligned along their long axis when a magnetic field is applied. Moreover, the magnetic torque and forces that can be exerted on them are higher in respect to the rectangular counterparts. Finally, cylindrical architectures experience lower drag forces during propulsion than rectangular ones.

A 10 μm thick layer of poly(ethylenglycol) diacrylate (PEGDA) was polymerized on the bottom of a 30 μm thick thermoresponsive, *N*-isopropylacrylamide-based layer (NIPAAM−AAM−PEGDA) to ensure a complete and multiwalled folding (Figure 1) upon swelling. The resulting cylindrical geometry had an average outer diameter of ∼0.6 mm and 2−3 folded layers, leading to a tight configuration. A comparison between the geometrical parameters of the open and closed configurations is reported in Table 1.

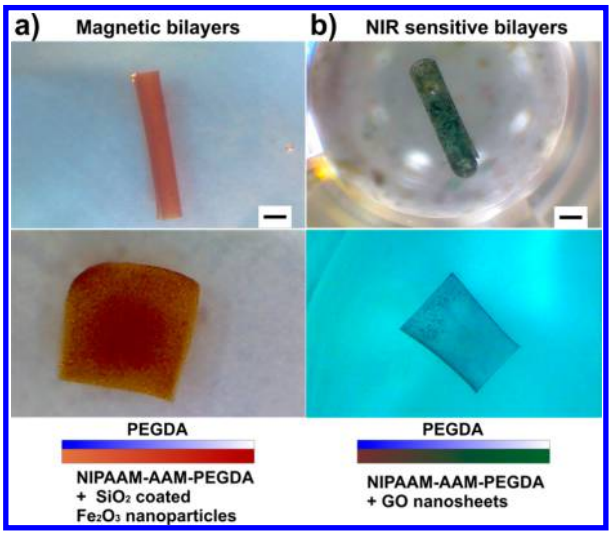

Figure 1. Tubular and rectangular configurations of (a) a magnetically responsive hydrogel nanocomposite containing silica coated iron oxide nanoparticles and (b) a NIR light-responsive hydrogel containing GO nanoparticles. Scale bar is 500 μm.

The properties of the external NIPAAM layer were tuned to have a high swelling ratio and a transition temperature around 40 °C. This was achieved by minimizing the quantity of cross-linker (PEGDA is limited to 0.4 mol %) and copolymerizing NIPAAM with relatively more hydrophilic AAM (15% in molar ratio). Additional features were achieved by dispersing silica-coated superparamagnetic nanoparticles or GO in the initial solution and by polymerizing them by UV light.

Table 1. Comparison of Geometrical Parameters of the Open and Closed Configurations of Self-Folding Cylinders[a]

	plate	hollow cylinder
volume	5.62×10^{-1} mm^3	5.62×10^{-1} mm^3
surface area	13.40 mm^2	6.72 mm^2
surface-to-volume ratio	23.8 mm^{-1}	11.9 mm^{-1}
layer thickness	90 μm	N/A
inner radius	N/A	135 μm
outer radius	N/A	290 μm

[a]Values were estimated from the initial geometry of the polymerized bilayer and from the images collected after swelling. Thickness of the single layer was not measured for the hollow cylinder due to lack of resolution of the images.

GO hydrogel nanocomposites have been recently introduced as low cost and biocompatible materials that are sensitive to NIR wavelength.[32,32] The NIR light is well-suited for in vivo applications because it can penetrate up to 10 cm into the tissues with minimal absorption by skin and blood vessels.[33] We have previously shown that hydrogel bilayers with dispersed GO sheets have a high sensitivity to optical stimulation, allowing fast kinetics of transition from the folded to the unfolded state.[26] The presence of GO partially modifies the swelling properties of the hydrogel formulation, but the temperature of transition remains the same.

Alternatively, silica-coated iron oxide nanoparticles were dispersed in the same matrix to produce magnetic nanocomposites and allow remote manipulation of the microtubes. The iron oxide nanoparticles (γ-Fe_2O_3) were produced by flame spray pyrolysis and were coated in situ with 23 wt % silica, following a previously established protocol.[34] The silica coating was employed to minimize their agglomeration and increase their biocompatibility and functionality.[35] Ultrasonication was used to disperse the magnetic nanoparticles in the NIPAAM copolymer solution. Five different concentrations (0.4, 1, 2, 4, and 8 wt %, related to γ-Fe_2O_3 content) were tested to optimize the trade-off between the magnetic properties of the nanocomposites and the drawbacks associated with the use of particles in the fabrication process. It is well-known that magnetic nanoparticles absorb UV light, which is responsible for the formation of radicals and the polymerization of the hydrogel solutions.[36] This limits the maximum thickness of nanocomposites, introduces localized defects, and forces a prolonged UV-exposure time. Additionally, the particle concentration influences the viscosity of the solutions, creating compatibility problems with the previously described fabrication method. We found that 6 min of UV exposure is sufficient to create uniform layers up to 180 μm thickness with nanoparticle concentrations up to 4 wt %. Composites with 8 wt % nanoparticles produced thinner layers with visible agglomerates on their surfaces.

The magnetic properties were analyzed with a vibrating sample magnetometer (VSM). The results revealed constricted hysteresis loops at room temperature (Figure 2a) with a small coercivity on the order of a few milliteslas. This can be ascribed to a mixed superparamagnetic−ferromagnetic behavior arising from the coexistence of isolated superparamagnetic nanoparticles together with interacting ferromagnetic-like nanoparticle agglomerates.[37] The saturation magnetization was found to be linearly proportional to the concentration of nanoparticles in the polymer film (Table 2 and Supporting Information, Figure S1). The value at 4 wt %, corresponding to a volumetric concentration of 1%, was found equal to 0.33 emu g^{-1}. This value confirms the expected filler loading level, as the saturation magnetization of the pure particle resulted in ∼30 emu g^{-1}. This concentration was chosen for the final self-folding prototype because it provided the best compromise between the performance of the microrobot (the final hydrogel based magnetic tubes were supposed to be steered by an electromagnetic manipulation system, having a maximum field of 50 mT and a field gradient of 5 T/m) and the already mentioned fabrication challenges.

The nanoparticle dispersibility in ethyl lactate, the solvent used for the preparation of the NIPAAM-based solutions, was

DOI: 10.1021/acsami.5b00181
ACS Appl. Mater. Interfaces 2015, 7, 6803−6811

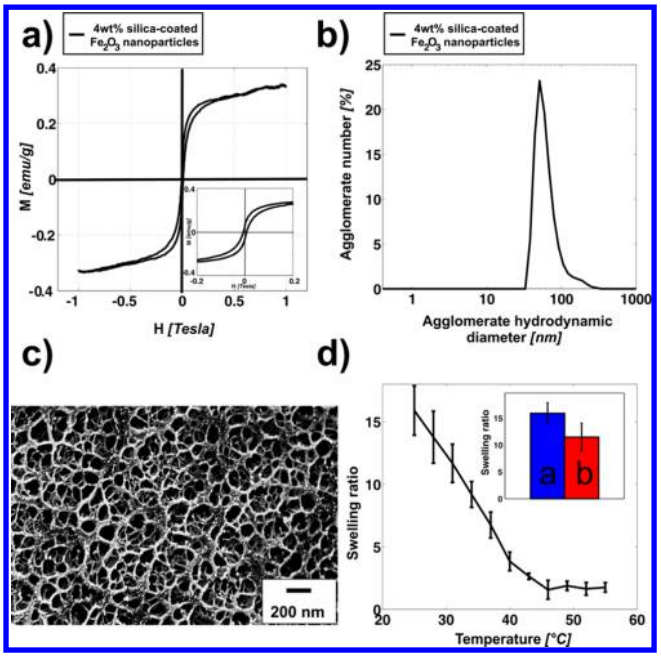

Figure 2. Characterization of magnetic nanocomposites. (a) Magnetic measurements of the 4 wt % nanocomposites show a constricted-type hysteresis loop which suggests the influence of interparticle magnetic dipolar interactions on the magnetic response of the composite material. (b) Representative curve of the number size distribution of a silica-coated Fe_2O_3 suspension in ethyl lactate by DLS, indicating the possibility to produce stable nanoparticle suspensions, which can be polymerized by UV light exposure. (c) The resulting hydrogels have a matrix pore size of ca. 100 nm; the nanoparticles can be seen as white dots entrapped in the fibers. (d) Swelling properties of the hydrogel composition show typical temperature dependence with a collapse state at around 42 °C. The introduction of nanoparticles (b bar) induces a significant decrease of the affinity to water, probably due to particle aggregation.

Table 2. Magnetization at 1 T of Hydrogel Nanocomposites Containing Silica-Coated Fe_2O_3 Nanoparticles at Various Concentrations, Measured by VSM

concentration (wt %)	specific saturation (emu/g)
0.4	0.02
1	0.06
2	0.142
4	0.329
8	0.658

characterized by dynamic light scattering (DLS) measurements. The average agglomerate hydrodynamic diameter for a 4 wt % ferrofluid was 145.8 ± 11.21 nm and a unimodal number size distribution with a mean value of 66.13 ± 28.46 nm was obtained (Figure 2b). These values indicate the presence of small agglomerations (the average primary particle diameter was calculated to be 24.1 ± 2.6 nm; see Supporting Information for calculation) which could not be broken with additional mixing methods. Nanocomposite solutions could, in any case, be prepared by ultrasonication and were stable for more than 1 day. Cryo-fixation was used to preserve the hydrated state of the nanocomposites and allowed imaging by SEM. As can be seen in Figure 2c, pores of the internal network of the size of ca. 100 nm are visible with a uniform distribution of the nanoparticles along the fibers of the matrix. No large agglomerates could be found during the imaging process, validating the used fabrication method.

Finally, the swelling properties of the nanocomposites were compared to nanoparticles-free hydrogel films. The results at equilibrium showed a decrease of 30% in the ability to incorporate water (Figure 2d). This result diverges from previous studies conducted on less concentrated nanocomposites.[38] This discrepancy could be explained by the prolonged UV exposure time, which increases cross-linking inside the matrix.[39] The lower swelling properties, as in the case of GO, did not influence the final design of the hydrogel-based microtubes, and they could achieve a closed-pack conformation with both fillers.

3.2. Magnetic Manipulation and Behavior of Magnetic Hydrogel Microrobots. Magnetic nanoparticles were embedded in the NIPAAM−AAM−PEGDA network of the bilayer to produce steerable magnetic nanocomposites. Magnetic hydrogels are particularly attractive because they offer the possibility to be actuated either by temperature, or by applying alternating magnetic fields, as previously described for similar materials.[40] 4 wt % of silica-coated γ-Fe_2O_3 nanoparticles were found to form layers with a high degree of particle dispersion and a sufficient level of magnetization for their magnetic manipulation. It is possible to generate different motions at the air−liquid interface or immersed in the liquid by magnetic control. It was found that the tubes were magnetized preferentially along their long axes, due to their shape anisotropy. The position and orientation of the structures were controlled by using magnetic field gradients lower than 0.2 T/m and magnetic fields lower than 20 mT (Supporting Information, video 1). The magnetic hydrogel-based microrobots were also subject to rapid changes of temperature to evaluate their conformation changes. As can be seen in Figure 3b, the bilayers were able to switch from a tubular to a rectangular configuration at around 40 °C, which corresponds to the transition temperature of the NIPAAM-based nanocomposites. The plate configuration switched to a tighter tube-like bilayer for temperatures higher than 50 °C. We are currently investigating the mechanism of this second folding phase.

The shape versatility of these hydrogels can be beneficial to modify on-demand the motion of these microdevices. A finite element method (FEM) analysis was performed to calculate the differences in the resistance to the translational motion of the microrobot, in an open (square) or closed (tube) configuration in a theoretical low Reynolds number flow. The calculation of drag forces was performed for a constant flow against a stationary microrobot, oriented along the direction of the flow (z direction) or perpendicular to it (y direction for the cylinder, xy direction for the plate). Differences could be found in general between the cylinder and the plate in both orientations (Figure 3c). The most significant data involved the cylinder oriented along the flow, and the plate perpendicular to it (two central bars in Figure 3c). The simulated drag constants doubled when passing from the "closed" (approximately 1.0×10^{-5} N/(m/s)) to the open configuration (2.4×10^{-5} N/(m/s), third bar in the graph), as a result of an increase of exposed surface area. We experimentally verified this significant change by measuring the velocity of robots with different folding states (Figure S4, Supporting Information). Tuning the hydrogels properties (and therefore the folding efficiency) or the external stimuli (magnetic fields, temperature, etc.) can further enhance this effect. This would eventually force the microrobot to lower

DOI: 10.1021/acsami.5b00181
ACS Appl. Mater. Interfaces 2015, 7, 6803−6811

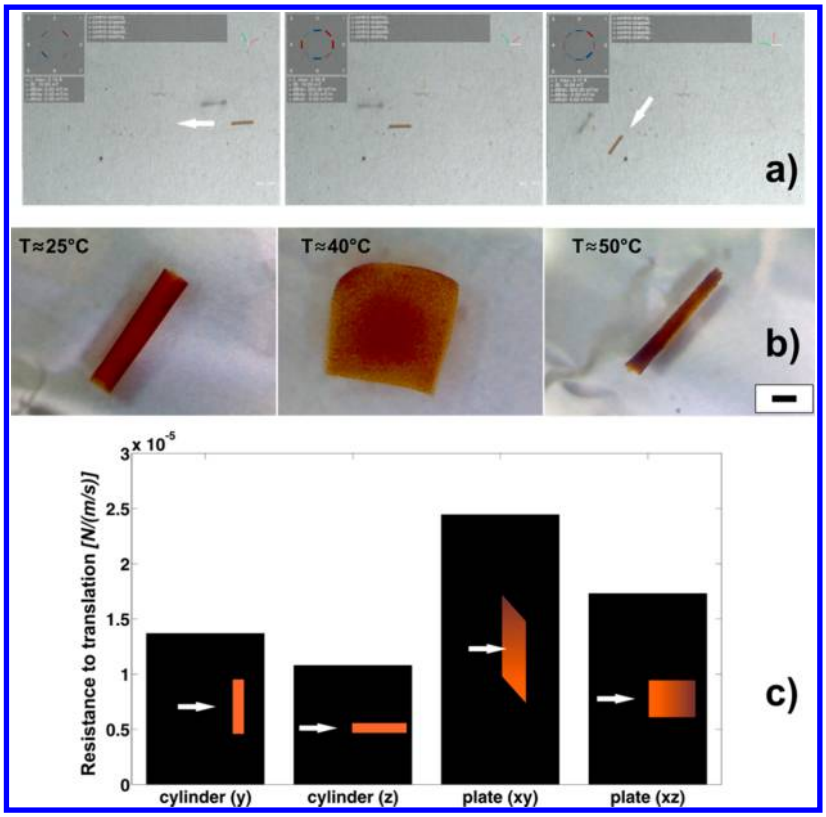

Figure 3. (a) Magnetic manipulation of a hydrogel microtube by means of the Octomag system. The white arrow indicates the direction of the applied field. (b) Shape transition of a rolled microtube, depending on the external temperature. At temperatures higher than 43 °C, the tube is capable of reaching a tighter conformation. Scale bar is 500 μm. (c) Results of the FEM-based simulation of the drag forces of self-folding tubes show that it is possible to significantly modify the motion of these structures in low Reynolds number flows. The white arrow indicates the direction of the fluid in respect to the orientation of the microrobot.

its speed or eventually stop in a specific position when activated. Moreover, a switch from a tubular shape to a more flat configuration could improve the distribution of drug delivery particles to tissues or to vessel walls due to an increase of contact area.[41]

3.3. Drug Delivery Experiments. GO-based NIR light responsive microtubes were fabricated in a way similar to the magnetic microrobot. After complete lyophilization, they were left swelling in a brilliant green (BG) dye solution, to mimic a loading process for a small hydrophilic drug. As the main part of their body was constituted by NIPAAM−AAM−PEGDA thermoresponsive nanocomposites, the same experimental procedure was performed also on small discs of this material. The structures were allowed to release the dye, and the release kinetics was monitored by spectrophotometry until no significant change in the signal could be recorded. NIR light was used to remotely induce collapse of the matrices, or change of shape, and the effect on the release kinetics was recorded and compared for both systems.

Depending on the physical and chemical properties of the polymer networks (size of the pores, functional binding sites, size and shape), and their affinity to the used model drug, the volume transition of similar hydrogel systems from a swollen to a collapsed state has been shown to induce higher[42−44] or reduced[45−47] release, when compared to a control experiment. Higher releases are mainly due to a "squeezing effect" that creates a convective motion of drug molecules out of the matrix, and to the aggregation of the hydrophobic polymer chains that creates open channels for a faster kinetics. Additionally, the chemical transition from a hydrophilic to a dominant hydrophobic conformation weakens the H-bonding interactions between the polymer and hydrophilic drugs, thus increasing their release. Opposite scenarios have been mainly attributed to the formation of a poorly permeable skin on the collapsed matrix, or to a significant decrease of the mesh size of the network, which is the representative parameter of the available space for diffusion.

GO single layers of NIPAAM copolymer were investigated for a period of 2 months in PBS. A set of samples, kept under constant stimulation of NIR light (785 nm) for the initial 2 h, showed a significantly (p = 0.005, from a one way ANOVA analysis) lower release rate (Figure 4a relative to the first 8 h of the experiment) than nonexposed samples used as control. The matrices appeared in a collapsed state (Figure 4b) for the duration of the experiment and released on average 30% less dye at the end of the first 2 h. A comparable release rate between the two systems was achieved only at the end of the first 8 h of experiments. However, the curves of absolute release revealed that this initial gap was not recovered, even after 2 months of experiment (Supporting Information, Figure S2).

A completely different scenario was observed when the hydrogel self-folding micro devices were taken into consideration and exposed to different cycles of NIR light (Figure 4c). Samples exposed to continuous stimulation changed their geometry, rapidly switching from a tubular state to an open square, thus increasing their surface area (Table 1 and Figure 4d). Despite the collapse of the light-responsive matrix, with presumably the same effects analyzed for the single layers, this

DOI: 10.1021/acsami.5b00181
ACS Appl. Mater. Interfaces 2015, 7, 6803−6811

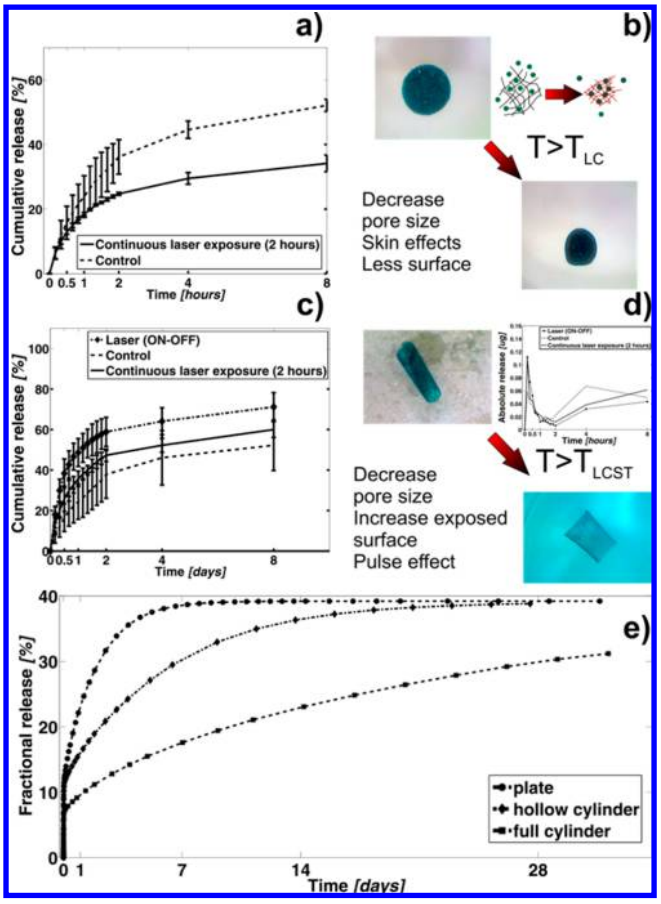

Figure 4. (a and b) Drug release kinetics of graphene oxide films exposed to IR light stimulation compared to control samples. The difference in the release can be explained by referring to the different phenomena happening during gel shrinking, including decrease of pore size, skin formation, and general decrease of surface area for diffusion. (c and d) Cumulative release from morphing hydrogel microdevices. The light responsive bilayers unfold from a wrapped to an open square configuration, therefore increasing the surface area responsible for drug diffusion. Despite the contraction of the hydrogel, the general effect is a temporary increase of drug release upon unfolding. The process can be tuned by changing the exposure type and duration. (e) Curves of fractional release of the cylinder and plate, as simulated by the FEM diffusion driven model. A full cylinder with the same volume could achieve a much more linear, zero-order like profile over time.

transition resulted in a significant increase (more than 20%) of the fractional release for the first 2 h ($p = 0.025$), followed by a sort of equilibrating phase in the following 2 h ($p = 0.07$ at the end of the 4 h), with the control samples releasing relatively more than the previously exposed samples.

These results are in good accordance with recent works performed in vivo with bigger nonresponsive hydrogel bilayers, thus confirming the potential of the shape changing devices.[21] Additionally, a more significant effect could be achieved by applying ON−OFF cycles (2 min ON, 2 min OFF) that forced the samples to alternatively open and close. This motion resulted in an increase of ca. 40% of the fractional release during the period of stimulation. The experiments were carried on for 1 month, until the release rate for every set of samples was close to zero (Supporting Information, Figure S2). Different from the single films of GO nanocomposites, the three sets of samples released a similar absolute amount of the dye at the end of the analyzed time frame, proving the nondestructive nature of the procedure of actuation.

To complete the analysis and study the sole effect of change in surface area, FEM-based simulations were run on different geometries: a hollow cylinder, a plate, and a full cylinder. The three models were built to have the same volume, initial concentration of drugs, diffusion coefficients, and boundary conditions. The simulations (Figure 4e) show the possibility to significantly modulate the drug release by shape change. The simulation condition is not reproducible in an experimental framework because a change of shape not only increases the surface area; it also decreases the pore size or collapses the bilayer (Figure 4d). The computational simulations show that if these unwanted effects could be minimized or completely eliminated, a significantly higher difference in the performance of different configurations would be observable. Nevertheless, one could imagine that by playing with shapes, material properties, and degree of imposed stimulus a favorable release profile in the intervention site and a conformation for minimal release during the trip could be achieved.

3.4. Shape-Changing Microhelices. The same fabrication method was used to produce shapes that are considered more advanced for microrobotic tasks. For example, helices have been shown to be optimal shapes for magnetic swimming microdevices at low Reynolds number regime.[48] When fabricated by self-folding techniques, and equipped with smart responsive hydrogels, a change of shape could be induced in order to have an optimal configuration for swimming and one

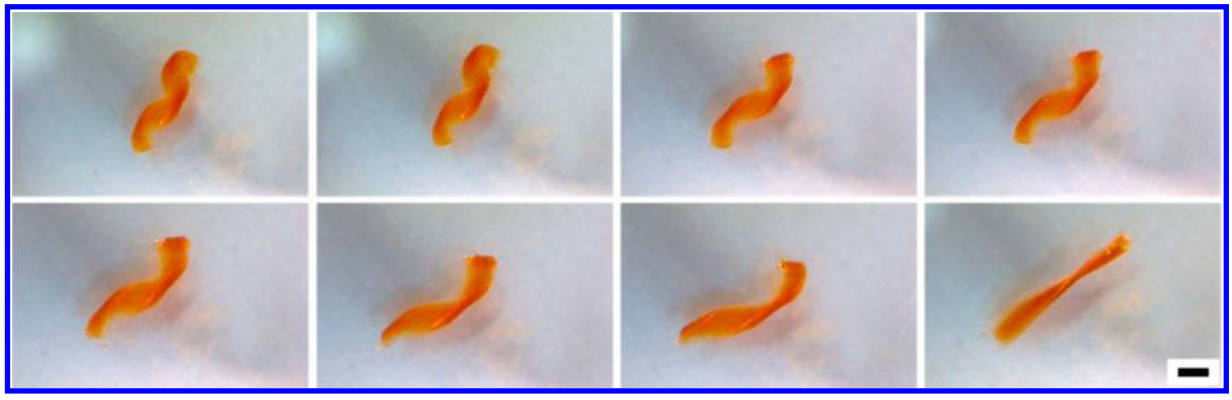

Figure 5. Temperature-dependent folding of a magnetic hydrogel ribbon. The temperature range is 20 °C, from (upper left) 25 °C to (lower right) 45 °C. Scale bar is 0.5 mm.

DOI: 10.1021/acsami.5b00181
ACS Appl. Mater. Interfaces 2015, 7, 6803−6811

not suitable for the same purpose. As an example, we propose change of shape of a magnetic, thermally responsive ribbon, fabricated in the same way as the rolled tubes (Figure 5). While the ribbons can corkscrew with rotating magnetic fields, tubular structures only rotate in place (Supporting Information, Figure S5 and videos 2 and 3). Despite not being optimized, one could imagine the possibility to achieve motion by rotating magnetic fields applied to the device in the first folded state. The same stimuli would not provide any net motion in the last flat configuration. Self-folding devices can also be combined with catalytic materials to perform self-propulsion inside biological microenvironments.[53,54]

4. CONCLUSIONS

In this work, we engineered self-folding smart microcarriers from magnetically and optically responsive hydrogel bilayers. Using on-demand shape change triggered by external light stimulation, we showed that the release kinetics of a model drug and the drag forces acting on the robots can be optimized according to the task. Shape morphing can be tailored by modifying the composition of the hydrogels, the geometrical design and the applied external stimuli. We fabricated structures that can perform a corkscrew motion in their folded state, and unfolding in response to changes in temperature results in loss of motility. This strategy opens up the possibility to program autonomous behavior by linking motility to microenvironmental conditions. The presented fabrication methodology, composite development, and wireless manipulation techniques combined with computational modeling form a complete platform for testing novel ideas for targeted therapies.

■ ASSOCIATED CONTENT

Supporting Information

Characterization of the magnetic properties of the nanocomposites, drug release kinetics of graphene oxide films exposed to NIR light, FEM models for drug delivery experiments and hydrodynamic forces acting on mobile microstructures, experimental investigation of the mobility of microstructures with different shapes and supplementary videos showing magnetic manipulation of hydrogel bilayers. This material is available free of charge via the Internet at http://pubs.acs.org.

■ AUTHOR INFORMATION

Corresponding Authors

* E-mail: jordi.sort@uab.cat.
* E-mail: sakarm@ethz.ch.

Notes

The authors declare no competing financial interest.

■ ACKNOWLEDGMENTS

Financial support by the European Research Council Advanced Grant "Microrobotics and Nanomedicine (BOTMED)", by the ERC grant agreement no. 247283, and by the Swiss National Science Foundation are gratefully acknowledged. Additionally, this work was supported by the National Institute of Health (R01 DE0013349). Dr. Eva Pellicer and Prof. Dr. Jordi Sort acknowledge 2014-SGR-1015 project from the Generalitat de Catalunya. Dr. Eva Pellicer is also grateful to MINECO for the "Ramon y Cajal" contract (RYC-2012-10839). A.S. and S.E.P. acknowledge financial support from the Swiss National Science Foundation (no. 200020-146176) and the European Research Council, under the European Union's Seventh Framework Programme (FP7/2007-2013, ERC grant agreement no. 247283). A.S. also acknowledges the Onassis Foundation for a student scholarship. The authors want also to acknowledge Falk Lucas, Stephan Handschin, and Dr. Roger Albert Wepf for the assistance in the use of the SEM facilities at EMEZ, ETH Zurich.

■ REFERENCES

(1) Mitragotri, S.; Lahann, J. Physical Approaches to Biomaterial Design. *Nat. Mater.* **2009**, *8*, 15−23.
(2) Jiang, W.; Kim, B. Y. S.; Rutka, J. T.; Chan, W. C. W. Nanoparticle-Mediated Cellular Response is Size-Dependent. *Nat. Nanotechnol.* **2008**, *3*, 145−150.
(3) Yoo, J.-W.; Doshi, N.; Miragotri, S. Adaptive Micro and Nanoparticles: Temporal Control over Carrier Properties to Facilitate Drug Delivery. *Adv. Drug. Del. Rev.* **2011**, *63*, 1247−1256.
(4) Balmert, S. C.; Little, S. R. Biomimetic Delivery with Micro- and Nanoparticles. *Adv. Mater.* **2012**, *24*, 3757−3778.
(5) Albanese, A.; Tang, P. S.; Chan, W. C. W. The Effect of Nanoparticle Size, Shape, and Surface Chemistry on Biological Systems. *Annu. Rev. Biomed. Eng.* **2012**, *14*, 1−16.
(6) Champion, J. A.; Katare, Y. K.; Mitragotri, S. Particle Shape: A New Design Parameter for Micro- and Nanoscale Drug Delivery Carriers. *J. Controlled Release* **2007**, *121*, 3−9.
(7) Champion, J. A.; Mitragotri, S. Role of Target Geometry in Phagocytosis. *Proc. Natl. Acad. Sci. U.S.A.* **2006**, *103*, 4930−4934.
(8) Gratton, S. E. A.; Ropp, P. A.; Pohlhaus, P. D.; Luft, J. C.; Madden, V. J.; Napier, M. E.; DeSimone, J. M. The Effect of Particle Design on Cellular Internalization Pathways. *Proc. Natl. Acad. Sci. U.S.A.* **2008**, *105*, 11613−11618.
(9) Geng, Y.; Dalhaimer, P.; Cai, S. S.; Tsai, R.; Tewari, M.; Minko, T.; Discher, D. E. Shape Effects of Filaments Versus Spherical Particles in Flow and Drug Delivery. *Nat. Nanotechnol.* **2007**, *2*, 249−255.
(10) Möller, J.; Luehmann, T.; Hall, H.; Vogel, V. The Race to the Pole: How High-Aspect Ratio Shape and Heterogeneous Environments Limit Phagocytosis of Filamentous *Escherichia coli* Bacteria by Macrophages. *Nano Lett.* **2012**, *12*, 2901−2905.
(11) Doshi, N.; Prabhakarpandian, B.; Rea-Ramsey, A.; Pant, K.; Sundaram, S.; Mitragotri, S. Flow and Adhesion of Drug Carriers in Blood Vessels Depend on Their Shape: A Study using Model Synthetic Microvascular Networks. *J. Controlled Release* **2010**, *146*, 196−200.
(12) Young, K. D. The Selective Value of Bacterial Shape. *Microbiol. Mol. Biol. R.* **2006**, *70*, 660−703.
(13) Kolhar, P.; Anselmo, A. C.; Gupta, V.; Pant, K.; Prabhakarpandian, B.; Ruoslahti, E.; Mitragotri, S. Using Shape Effects to Target Antibody-Coated Nanoparticles to Lung and Brain Endothelium. *Proc. Natl. Acad. of Sci. U.S.A.* **2013**, *110*, 10753−10758.
(14) Behl, M.; Lendlein, A. Shape-Memory Polymers. *Mater. Today* **2007**, *10*, 20.
(15) Chaterji, S.; Kwon, I. K.; Park, K. Smart Polymeric Gels: Redefining the Limits of Biomedical Devices. *Prog. Polym. Sci.* **2007**, *32*, 1083−1122.
(16) Peppas, N. A.; Hilt, J. Z.; Khademhosseini, A.; Langer, R. Hydrogels in Biology and Medicine: From Molecular Principles to Bionanotechnology. *Adv. Mater.* **2006**, *18*, 1345−1360.
(17) Ionov, L. Soft Microorigami: Self-Folding Polymer Films. *Soft Matter* **2011**, *7*, 6786−6791.
(18) Randall, C. L.; Gultepe, E.; Gracias, D. H. Self-Folding Devices and Materials for Biomedical Applications. *Trends Biotechnol.* **2012**, *30*, 138−146.
(19) Fernandes, R.; Gracias, D. H. Self-Folding Polymeric Containers for Encapsulation and Delivery of Drugs. *Adv. Drug Deliver. Rev.* **2012**, *64*, 1579−1589.
(20) Ionov, L. Biomimetic Hydrogel-Based Actuating Systems. *Adv. Funct. Mater.* **2013**, *23*, 4555−4570.

DOI: 10.1021/acsami.5b00181
ACS Appl. Mater. Interfaces 2015, 7, 6803−6811

(21) Baek, K.; Jeong, J. H.; Shkumatov, A.; Bashir, R.; Kong, H. In Situ Self-Folding Assembly of a Multi-Walled Hydrogel Tube for Uniaxial Sustained Molecular Release. *Adv. Mater.* **2013**, *25*, 5568−5573.
(22) Pedron, S.; van Lierop, S.; Horstman, P.; Penterman, R.; Broer, D. J.; Peeters, E. Stimuli Responsive Delivery Vehicles for Cardiac Microtissue Transplantation. *Adv. Funct. Mater.* **2011**, *21*, 1624−1630.
(23) Zakharchenko, S.; Puretskiy, N.; Stoychev, G.; Stamm, M.; Ionov, L. Temperature Controlled Encapsulation and Release using Partially Biodegradable Thermo-Magneto-Sensitive Self-Rolling Tubes. *Soft Matter* **2010**, *6*, 2633−2636.
(24) Gultepe, E.; Randhawa, J. S.; Kadam, S.; Yamanaka, S.; Selaru, F. M.; Shin, E. J.; Kalloo, A. N.; Gracias, D. H. Biopsy with Thermally-Responsive Untethered Microtools. *Adv. Mater.* **2013**, *25*, 514−519.
(25) Xi, W.; Solovev, A. A.; Ananth, A. N.; Gracias, D. H.; Sanchez, S.; Schmidt, O. G. Rolled-up Magnetic Microdrillers: Towards Remotely Controlled Minimally Invasive Surgery. *Nanoscale* **2013**, *5*, 1294−1297.
(26) Fusco, S.; Sakar, M. S.; Kennedy, S.; Peters, C.; Bottani, R.; Starsich, F.; Mao, A.; Sotiriou, G. A.; Pane, S.; Pratsinis, S. E.; Mooney, D.; Nelson, B. J. An Integrated Microrobotic Platform for On-Demand, Targeted Therapeutic Interventions. *Adv. Mater.* **2014**, *26*, 952−957.
(27) Kummer, M. P.; Abbott, J. J.; Kratochvil, B. E.; Borer, R.; Sengul, A.; Nelson, B. J. OctoMag: An Electromagnetic System for 5-DOF Wireless Micromanipulation. *IEEE T. Robot.* **2010**, *26*, 1006−1017.
(28) Huang, T.-Y.; Qiu, F.; Tung, H.-W.; Peyer, K. E.; Shamsudhin, N.; Pokki, J.; Zhang, L.; Chen, X.-B.; Nelson, B. J.; Sakar, M. S. Cooperative Manipulation and Transport of Microobjects Using Multiple Helical Microcarriers. *RSC Adv.* **2014**, *4*, 26771−26776.
(29) Peters, C.; Fusco, S.; Li, Y.; Kuhne, S.; Nelson, B. J.; Hierold, C. Backside Liquid Phase Photolithography for Fabricating Self-Organizing Hydrogel Bilayers. *Eurosensor* **2012**, *47*, 1219−1222.
(30) Zakharchenko, S.; Sperling, E.; Ionov, L. Fully Biodegradable Self-Rolled Polymer Tubes: A Candidate for Tissue Engineering Scaffolds. *Biomacromolecules* **2011**, *12*, 2211−2215.
(31) Zhu, C. H.; Lu, Y.; Peng, J.; Chen, J. F.; Yu, S. H. Photothermally Sensitive Poly(*N*-isopropylacrylamide)/Graphene Oxide Nanocomposite Hydrogels as Remote Light-Controlled Liquid Microvalves. *Adv. Funct. Mater.* **2012**, *22*, 4017−4022.
(32) Lo, C. W.; Zhu, D. F.; Jiang, H. R. An Infrared-Light Responsive Graphene-Oxide Incorporated Poly(*N*-isopropylacrylamide) Hydrogel Nanocomposite. *Soft Matter* **2011**, *7*, 5604−5609.
(33) Weissleder, R. A Clearer Vision for in Vivo Imaging. *Nat. Biotechnol.* **2001**, *19*, 316−316.
(34) Teleki, A.; Suter, M.; Kidambi, P. R.; Ergeneman, O.; Krumeich, F.; Nelson, B. J.; Pratsinis, S. E. Hermetically Coated Superparamagnetic Fe_2O_3 Particles with SiO_2 Nanofilms. *Chem. Mater.* **2009**, *21*, 2094−2100.
(35) Lu, A. H.; Salabas, E. L.; Schuth, F. Magnetic Nanoparticles: Synthesis, Protection, Functionalization, and Application. *Angew. Chem., Int. Ed.* **2007**, *46*, 1222−1244.
(36) Damean, N.; Parviz, B. A.; Lee, J. N.; Odom, T.; Whitesides, G. M. Composite Ferromagnetic Photoresist for the Fabrication of Microelectromechanical Systems. *J. Micromech. Microeng.* **2005**, *15*, 29.
(37) Nogues, J.; Skumryev, V.; Sort, J.; Stoyanov, S.; Givord, D. Shell-Driven Magnetic Stability in Core−Shell Nanoparticles. *Phys. Rev. Lett.* **2006**, *97*, 157203.
(38) Marklein, R. A.; Burdick, J. A. Spatially Controlled Hydrogel Mechanics to Modulate Stem Cell Interactions. *Soft Matter* **2010**, *6*, 136−143.
(39) Sunyer, R.; Jin, A. J.; Nossal, R.; Sackett, D. L. Fabrication of Hydrogels with Steep Stiffness Gradients for Studying Cell Mechanical Response. *PLoS One* **2012**, *7*, e46107.
(40) Satarkar, N. S.; Hilt, J. Z. J. Magnetic Hydrogel Nanocomposites for Remote Controlled Pulsatile Drug Release. *J. Controlled Release* **2008**, *130*, 246−251.
(41) Decuzzi, P.; Pasqualini, R.; Arap, W.; Ferrari, M. Intravascular Delivery of Particulate Systems: Does Geometry Really Matter? *Pharm. Res.* **2009**, *26*, 235−243.
(42) Ma, X.; Dong, L.; Ji, X.; Li, Q.; Gou, Y.; Fan, X.; Wang, M.; Di, Y.; Deng, K. Drug Release Behaviors of a pH/Thermo-Responsive Porous Hydrogel from Poly(*N*-acryloylglycinate) and Sodium Alginate. *J. Sol−Gel Sci. Technol.* **2013**, *68*, 356−362.
(43) Deng, K.; Zhong, H.; Zheng, X.; Song, X.; Tian, H.; Zhang, P.; Ren, X.; Wang, H. Synthesis, Characterization, and Drug Release Behaviors of a Novel Thermo-Sensitive Poly(*N*-acryloylglycinates). *Polym. Adv. Technol.* **2010**, *21*, 584−590.
(44) Bae, Y.; Okano, T.; Kirn, S. "On−Off" Thermocontrol of Solute Transport. II. Solute Release from Thermosensitive Hydrogels. *Pharm. Res.* **1991**, *8*, 624−628.
(45) Satarkar, N. S.; Hilt, J. Z. Hydrogel Nanocomposites as Remote-Controlled Biomaterials. *Acta Biomater.* **2008**, *4*, 11−16.
(46) Brazel, C. S.; Peppas, N. A. Pulsatile Local Delivery of Thrombolytic and Antithrombotic Agents using Poly(*N*-isopropylacrylamide-co-methacrylic acid) Hydrogels. *J. Controlled Release* **1996**, *39*, 57−64.
(47) Dinarvand, R.; D'Emanuele, A. The Use of Thermoresponsive Hydrogels for On−Off Release of Molecules. *J. Controlled Release* **1995**, *36*, 221−227.
(48) Peyer, K. E.; Zhang, L.; Nelson, B. J. Bio-inspired Magnetic Swimming Microrobots for Biomedical Applications. *Nanoscale* **2013**, *5*, 1259−1272.
(49) Kovtyukhova, N. I.; Ollivier, P. J.; Martin, B. R.; Mallouk, T. E.; Chizhik, S. A.; Buzaneva, E. V.; Gorchinskiy, A. D. Layer-by-Layer Assembly of Ultrathin Composite Films from Micron-Sized Graphite Oxide Sheets and Polycations. *Chem. Mater.* **1999**, *11*, 771−778.
(50) Peyer, K.; Siringil, E.; Zhang, L.; Suter, M.; Nelson, B. Superparamagnetic Microrobots: Fabrication by Two-Photon Polymerization and Biocompatibility. In *Biomimetic and Biohybrid Systems*, Vol. *8064*; Lepora, N.; Mura, A., Krapp, H., Verschure, P. M. J., Prescott, T., Eds.; Springer: Berlin Heidelberg, 2013, pp 216−227.
(51) Marino, H.; Bergeles, C.; Nelson, B. J. *Robust H ∞ Control for Elextromagnetic Steering of Microrobots*. In Proceedings of the 2012 IEEE International Conference on Robotics and Automation, St. Paul, MN, May 14−18, 2012; IEEE: New York, NY,201224982503
(52) Happel, J.; Brenner, H. *Low Reynolds Number Hydrodynamics*, Vol. *1*, Springer: Netherlands, The Hague, 1983.
(53) Magdanz, V.; Stoychev, G.; Ionov, L.; Sanchez, S.; Schmidt, O. G. Stimuli-Responsive Microjets with Reconfigurable Shape. *Angew. Chem., Int. Ed.* **2014**, *53*, 2673−2677.
(54) Sánchez, S.; Soler, L.; Katuri, J. Chemically Powered Micro- and Nanomotors. *Angew. Chem., Int. Ed.* **2015**, *54*, 1414−1444.

DOI: 10.1021/acsami.5b00181
ACS Appl. Mater. Interfaces 2015, 7, 6803−6811